Design a wearable device for return-to-run rehabilitation military soldiers

Alshaimaa Azzam Ibrahim, Hesham Eldesoky Elsheikh
Minia University, Egypt, elshimaaazam@gmail.com, heshamelsheikh72@gmail.com

Supervisor: Mohamed Abdelhady, Wael Abouelwafa Ahmed
Cleveland State University, Cleveland, m.abdelelhadi@csuohio.edu, Minia University, Egypt, ORCD ID: 0000-0001-7449-8014

***Abstract*— Since there are numerous sectors for patients with walking difficulties, such as stroke, sports, and medical rehabilitation, the study of human gait analysis has been an important endeavor for years. However, such research necessitates the use of equipment that can precisely quantify the movement of body parts. This paper outlines a development strategy for a small wireless internet of things (IoT) board, from embedded system design to kinematic data collection. The goal of this project is to develop an acquisition IoT board that can measure and collect the knee, hip, and ankle angles of a healthy person as well as a patient with certain diseases. An enclosure designed to house the board and its associated battery forms a wearable unit that can be attached to the lower limbs of humans. The electronic board design establishes an inner communication between a high-fidelity inertial measurement unit (IMU) and a microcontroller, as well as an outer communication between the microcontroller and the radio frequency (RF) module. The board design considers a bidirectional radio communication, though multiple boards are able to share, exchange, and pass IMU data to a personal computer as well.**

Keywords—gait analyses, PD-AFO, IMU, PCB Design

I. INTRODUCTION

Lower extremity fractures provide a significant portion of the total reported military injuries and can completely derail a military service member's or soldier's career. After their injuries, some service members experience debilitating pain and functional deficits, and they are unable to return to their previous level of function, which may prevent them from returning to active duty.

After a severe musculoskeletal lower extremity injury, a service member can return to high-level functional activities such as walking on uneven terrains, stair climbing, and so on, by combining a passive-dynamic ankle-foot orthosis (PD-AFO) with a specialized return-to-run rehabilitation program. [[1],[2] ,[3], [4],[5]].

We were also interested in how the kinematics and functional outcomes of patients who used the PD-AFO while running, which is how the PD-AFO was designed to be used, differed from a group of uninjured controls. Because rehabilitation includes strength and endurance training as well as understanding what is pathological and different about an injured service member's gait at self-selected running speeds compared to an uninjured runner, this is an interpersonal skill. Identifying differences is the next step in improving each service member's running technique and ability. This could potentially help them meet their goals and make the most of their brace. As a result, a variety of sensors (such as IMUs) are employed. [[6],[7]], Sensors for electromyography (EMG) [[8]-[9]]. In terms of control requirements, gait phase detection has been adopted.

The most basic gait phase-detection methods rely on identifying peaks and threshold rules, while more advanced methods employ machine learning techniques. IMU-based approaches were found to be more suitable for long-term use than force sensors. Martinez-Hernandez et al. proposed Convolutional Neural Networks (CNN) to detect gait phase. Gait characteristic parameters can be extracted using convolution kernels for classification, resulting in high gait phase detection accuracy[10]. Saikat Sahoo et al. proposed using nine rules to detect gait phases to solve the time delay problem of IMUs in detecting gait phases [11]. The Vicon-system is frequently used as training label data and a reference for validations due to its high accuracy and short time difference.

There are three common evaluation indicators in the field of gait phase detection. (1) Detection time: the amount of time it takes to compute the output. (2) Detection accuracy: This indicator is calculated using the percentage of false or true detection phases (3) Time difference: The difference in time between the temporal phases detected by the reference device, such as footswitches, force sensors, or a vicon-system. Despite the fact that the current state-of-the-art gait detection method has an accuracy rate of more than 90%, the control system must account for a time difference [12]. Our goal is to achieve high detection accuracy while minimizing time difference.

The implementation goal of our work is to improve the ability of people who wear (PD-AFO) to perform heavy physical labor, such as soldiers transporting military supplies in high altitude areas and couriers in the logistics industry, among others. It is critical to detect the gait phase quickly and accurately in real-time in order to achieve practical powered (PD-AFO) in a complex environment. In addition, for soldiers in force training who use the treadmill, a doctor's complete gait analysis is provided (PD-AFO).

The following is how the rest of the paper is structured: Section II outlines the methodology for gait analysis with IMU that has been proposed. Section III discusses the IoT system's main hardware components. Section IV discusses the design of the prosthesis's total rotation. as well as data collection instrumentation Section V includes a conclusion as well as suggestions for future work.

II. METHODOLOGY

In this paper we show the design of a compact module to monitor lower limb kinematics. Although, designing a compact wireless inertial measurement module would help to provide a fidelity measurement wirelessly, using prototyped kits boards like Arduino does not provide the minimum accuracy and increases the difficulty of attaching the combined modules to human body. Also, design a customizable hardware from scratch is a challenging problem. For example, IoT embedded system design that include wireless capabilities needs to tune special specs. The tuning process is a hard trails and error process. These difficulties increase with considering extra compactness to shrink down the design size.

Using the distributed embedded system notion, The PCB serves as a single node in a perspective wireless sensory network (WSN), which it can attach to any human body segment. This prospective constraint with an important design requirement. Standard design cycle depicted by Figure 1 has been considered to achieve design goals. The design cycle comprises three main phases: the design phase to skitch the shape of embedded system prototype. Altium software used to design the different layers of PCB. At the prototyping phase the design sends to be manufactured, then visually inspected after receiving prototyped design. Finally, in the test phase the hardware functionally tested, and the captured signal compared with Winter standard signals.

The first Node is located at the first link's end and measures the orientation of this link to the base frame, and the second Node is located at the second link's end and measures the orientation of the second link to the base frame, as shown in figure (1), where θ_1 refers to the thigh angle, , θ_2 refers to the shank angle, and $\theta_3$refers to the *knee* angle. It should be noted that the sensors' directions are kept the same.

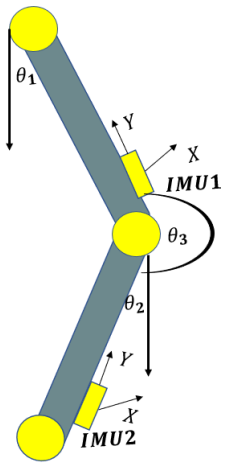

Fig 1. Model of IMU sensors on lower Limbs

III. DESIGN DESCRIPTION

A. *Hardware Components*

The hardware part comprises a central microcontroller ATMEGA328P-AU, a low-power, CMOS 8-bit microcontroller based on enhanced reduced instruction set (RISC) architecture with 32K bytes of in-system programmable; the microcontroller is equipped with a programmable watchdog timer which has an internal oscillator. The second main component is the triple-phase bridge. This is a bridge configuration of six MOSFETs used to power the motor's coils. Each of these MOSFETs is controlled by the IR2101, which is a dual driver capable of controlling both the high and low sides of the bridge. The inertial measurement unit (IMU) MPU-6050, which combines a gyroscope and an accelerometer, is the third major component. For gyroscopic and acceleration measurements, both used the I2C protocol.

The board is used to control brushless motors; in this case, the motor has a triple-phase input. To control this input, a particular sequence of LOWs and HIGHs signals must be applied in a predefined order where it uses Triple phase MOSFET bridge control to energize the coils of the motor.

The prototype has many advantages, including a small physical dimension, flexibility, and BEMF voltage dividers, where the voltage from the motor is greater than the maximum voltage that the ATMEGA328P-AU can accept as input, in this case, 5V. So, using 10K and 33K resistors, we reduced the voltage so that the ATmega328's analogue input could read it. This input will be used to detect the rotor's position and determine when to move on to the next step of the rotating sequence. We also have the ATmega328 microcontroller and the CH340 programmer, which can be used to upload code via the USB connector.

B. PCB design

The designed PCB is 65x35 mm. with a thickness of 1.6 mm, signal tracks are 0.2 mm to conductor current (0.59 Amp), and power tracks are 2.54 mm to conductor current (3 Amp). the design consists of four layers is divide into Signals layers, Power, and ground layers. {Signals /GND / Power /Signals}. Figure 2 shows the system top layer for the designed four-layer PCB.

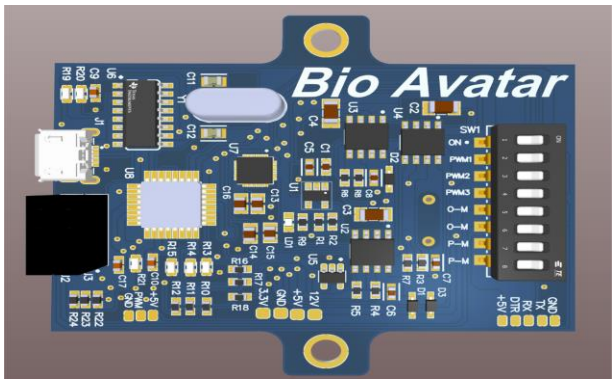

Fig 2. Top Layer Designed PCB Board.

The ground layer should always be adjacent (and close to) the upper signal layer to minimize electromagnetic radiation and crosstalk. And the power layer should also be adjacent (and close to) the ground layer as this adds inter-plane capacitance, which helps minimize power supply noise.

The power (VCC) plane is divided into three sections (3.3V, 5V, and 12V), with components physically placed in various locations on the board. Splitting the power plane into separate areas can be used to eliminate common return paths, where the design constraints are illustrated in Table I show the rules to follow while designing the trace width varies from 0.15 mm to 2.54 for signal and power traces, respectively, and is considered one of the most critical design parameters during the PCB design.

Table I. Multilayer PCB design characteristics.

Specs	Unit	Signal trace	Power trace
Trace width	mm	0.15	2.54
Conductor current	Amps	0.5	3
Voltage drop	V	0.03	0.01
Power dissipation	W	0.017	0.03
Resistance	Ohm	0.06	0.004
Track clearance	mm	0.3	0.3
Voltage between conductors	V	3.3-5-12	3.3-5-12
Plating thickness	mm	1	2
Layer set	layer	4	NaN

IV. INSTRUMENTATION AND DATA COLLECTION

Figure 3 depicts the hip joint's motion. During the terminal swing (phase 3), maximum hip flexion occurs, followed by a slight extension prior to initial contact (phase 1). The hip extends after initial contact (phase 1) as the body rotates 150 degrees per second over the limb. After opposite foot strike (phase 2), the trailing limb begins to flex at the hip, and weight is transferred to the forward limb. This is the period prior to the start of the swing. At 60 percent of the gait cycle, the toe leaves the ground, and the hip flexes quickly at 200 degrees per second. The slope of the angle against the time plot below shows that the limb is progressing forward and preparing for the next initial contact (phase 1).

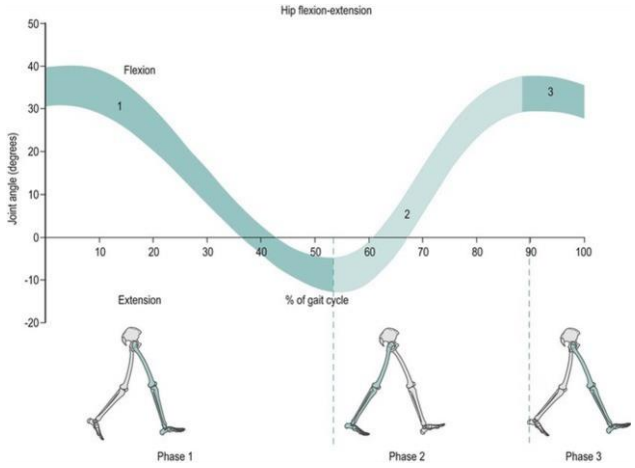

Fig 3. Hip Joint Cycle

During gait, the knee joint uses the sagittal, transverse, and coronal planes. Most of the knee joint motion occurs in the sagittal plane, which includes flexion and extension of the knee joint. The flexion and extension of the knee joint is cyclic, ranging from 0 to 70 degrees, though the amount of peak flexion varies. Walking speed, subject individuality, and the landmarks used to designate limb segment alignments could all play a role. There are five phases, as shown in figure 4.

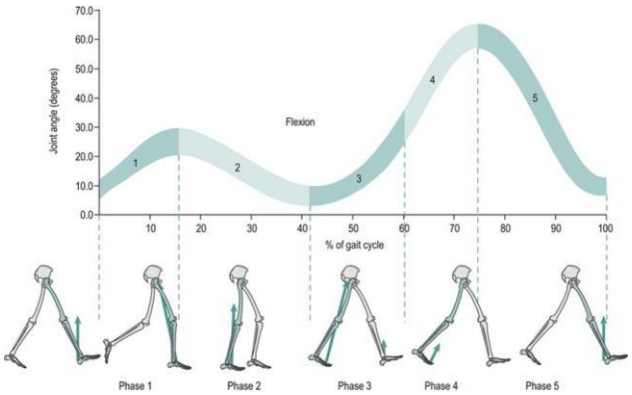

Fig 4. Knee Joint Cycle

Thigh rotation represents the rotation of the hip (eq 1), but the shank rotation represents the sum of the knee and hip rotations (eq 2), where the knee angle can be calculated as in eq 3.

$$R_{Hip} = R_{Thigh} \quad (1)$$
$$R_{Shank} = R_{Thigh} + R_{Hip} \quad (2)$$
$$Knee\ Angle = 180 + R_{Shank} \quad (3)$$

In order to calculate the total rotation matrix in 3d space equation 4 can be used for each joint to calculate the torque and acceleration for the exoskeleton.

$$R_x R_y R_z = \begin{pmatrix} C(\gamma)\,C(\beta) & -S(\gamma)\,C(\alpha) + C(\gamma)\,S(\beta)\,S(\alpha) & S(C)\,S(\alpha) + C(\gamma)\,S(\beta)\,C(\alpha) \\ C(\gamma)\,C(\beta) & C(\gamma)\,C(\alpha) + S(\gamma)\,S(\beta)\,S(\alpha) & -C(\gamma)\,S(A) + S(\gamma)\,S(\beta)\,C(A) \\ -S(B) & C(B)\,S(\alpha) & C(B)\,C(\alpha) \end{pmatrix} \quad \text{-----(4)}$$

Where (C) denotes cosine and (S) denotes sine of the respective angles. α, β, γ which are the rotation angles around x, y, and z respectively.

This paper explains how to collect and make analysis to IMU data in order to detect an abnormal gait caused by lower limbs motion. The system configuration is shown in Figure 5, which includes two IMU sensors for each leg to create a network topology of joints and links for the human leg. The study employs NRF technology to transmit data wirelessly. The Shank node sends data to the thigh node for each leg, which then sends all data to the receiver node connected to the computer for processing and storage. This configuration records the system's high accuracy and short delay time.

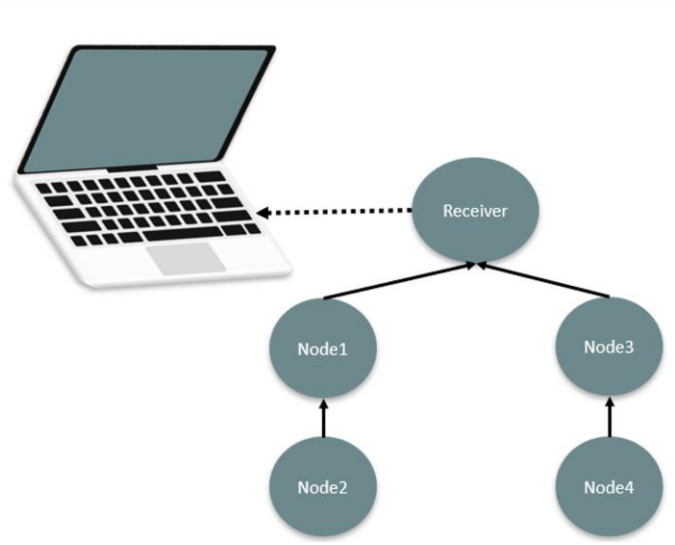

Fig 5. Network System

V. RESULTS

The interaction of many body systems, including coordination, sensation, and strength, is required for normal gait. Aging, for example, is a growing public health concern around the world. When ageing causes weakness in strength and sensation, the interacting systems can lead to gait or walking abnormality. This section presents a preliminary experimental result for recognising normal and abnormal gait types from hip and knee joint angles. Figure 6 (a) represents a sample of the measured thigh and shank angles using IMU sensors. Figure 6(b) shows the calculated knee angle.

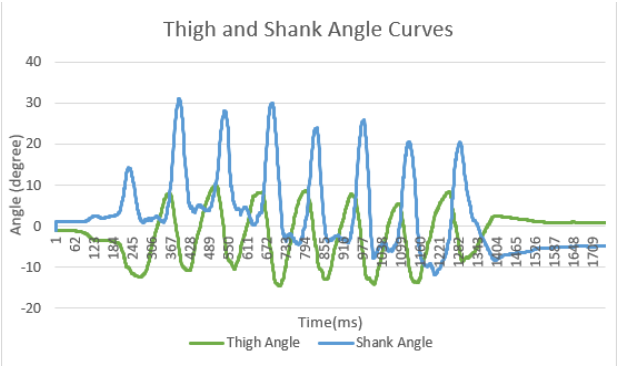

Fig 6. (a) Thigh and Shank Angle Curves

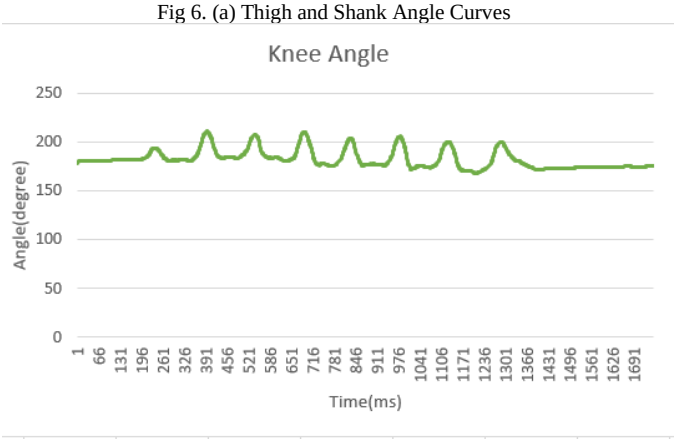

Fig 6. (b) Knee Angle Curve

The Battery used for the experiment was a Nokia battery. It has been tested to calculate the discharging duration to know the maximum period of investigation, and it was about 5 hours. figure 7 shows the discharging rate for the Battery used.

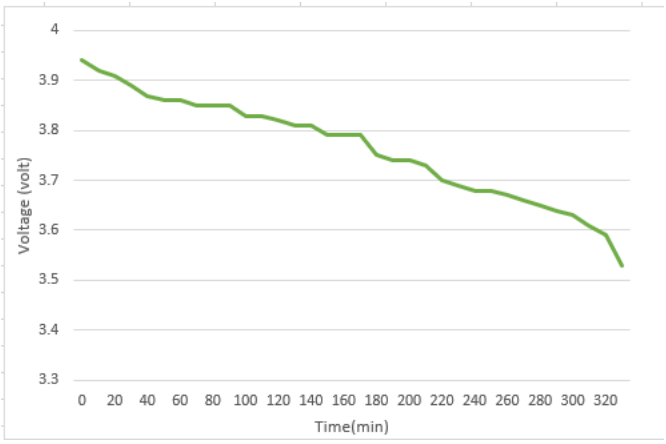

Fig 7. Battery discharging curves

VI. CONCLUSIONS

In this paper, we describe the design and development process for a small IoT hardware module. This module would be extremely useful for therapists and human motion analysts who want to assess human motion using high-fidelity electronic components. The methodology for overcoming design challenges is presented by selecting a convenient design configuration prior to the prototyping phase. The strategy includes selecting normal and power traces to overcome electromagnetic noise, which affects the wireless capability of IoT devices. Additionally, vias are configured to maximize module compactness.

The IoT module was tested to measure a human subject's knee angle, and the resulting waveform was compared to Winter's recorded data. Aside from the ease of attachment to the human body provided by the module's compactness, the module demonstrates promising capabilities for capturing human motion. Our upcoming projects Adding more capabilities to this IoT module and apply data gathering protocol for different types of patients.

REFERENCES

[1] J. A. Blair, J. C. Patzkowski, R. V. Blanck, J. G. Owens, and J. R. Hsu, "Return to duty after integrated orthotic and rehabilitation initiative," *J. Orthop. Trauma*, vol. 28, no. 4, pp. 70–74, 2014, doi: 10.1097/BOT.0000000000000006.

[2] W. Dite and V. A. Temple, "A clinical test of stepping and change of direction to identify multiple falling older adults," *Arch. Phys. Med. Rehabil.*, vol. 83, no. 11, pp. 1566–1571, 2002, doi: 10.1053/apmr.2002.35469.

[3] J. R. Hsu *et al.*, "Patient response to an integrated orthotic and rehabilitation initiative for traumatic injuries: The PRIORITI-MTF study," *J. Orthop. Trauma*, vol. 31, no. 4, pp. S56–S62, 2017, doi: 10.1097/BOT.0000000000000795.

[4] J. C. Patzkowski *et al.*, "Comparative effect of orthosis design on functional performance," *J. Bone Jt. Surg. - Ser. A*, vol. 94, no. 6, pp. 507–515, 2012, doi: 10.2106/JBJS.K.00254.

[5] B. K. Potter *et al.*, "Multisite evaluation of a custom energy-storing carbon fiber orthosis for patients with residual disability after lower-limb trauma," *J. Bone Jt. Surg. - Am. Vol.*, vol. 100, no. 20, pp. 1781–1789, 2018, doi: 10.2106/JBJS.18.00213.

[6] H. M. Schepers, E. H. F. Van Asseldonk, C. T. M. Baten, and P. H. Veltink, "Ambulatory estimation of foot placement during walking using inertial sensors," *J. Biomech.*, vol. 43, no. 16, pp. 3138–3143, 2010, doi: 10.1016/j.jbiomech.2010.07.039.

[7] R. Schwesig, S. Leuchte, D. Fischer, R. Ullmann, and A. Kluttig, "Inertial sensor based reference gait data for healthy subjects," *Gait Posture*, vol. 33, no. 4, pp. 673–678, 2011, doi: 10.1016/j.gaitpost.2011.02.023.

[8] K. Kiguchi and Y. Hayashi, "An EMG-based control for an upper-limb power-assist exoskeleton robot," *IEEE Trans. Syst. Man, Cybern. Part B Cybern.*, vol. 42, no. 4, pp. 1064–1071, 2012, doi: 10.1109/TSMCB.2012.2185843.

[9] S. Kyeong, W. Shin, M. Yang, U. Heo, J. rou Feng, and J. Kim, "Recognition of walking environments and gait period by surface electromyography," *Front. Inf. Technol. Electron. Eng.*, vol. 20, no. 3, pp. 342–352, 2019, doi: 10.1631/FITEE.1800601.

[10] U. Martinez-Hernandez, A. Rubio-Solis, and A. A. Dehghani-Sanij, "Recognition of Walking Activity and Prediction of Gait Periods with a CNN and First-Order MC Strategy," *Proc. IEEE RAS EMBS Int. Conf. Biomed. Robot. Biomechatronics*, vol. 2018-August, pp. 897–902, 2018, doi: 10.1109/BIOROB.2018.8487220.

[11] S. Sahoo, M. Saboo, D. K. Pratihar, and S. Mukhopadhyay, "Real-Time Detection of Actual and Early Gait Events during Level-Ground and Ramp Walking," *IEEE Sens. J.*, vol. 20, no. 14, pp. 8128–8136, 2020, doi: 10.1109/JSEN.2020.2980863.

[12] H. T. T. Vu *et al.*, "A review of gait phase detection algorithms for lower limb prostheses," *Sensors (Switzerland)*, vol. 20, no. 14, pp. 1–19, 2020, doi: 10.3390/s20143972.